

Probing quark-lepton correlation in GUTs with high-precision neutrino measurements

Zi-Qiang Chen ^{1,2,3} Gao-Xiang Fang ^{1,2,3} and Ye-Ling Zhou ¹

¹*School of Fundamental Physics and Mathematical Sciences,
Hangzhou Institute for Advanced Study, UCAS, Hangzhou 310024, China*

²*Institute of Theoretical Physics, Chinese Academy of Sciences, Beijing 100190, China*

³*University of Chinese Academy of Sciences, Beijing 100049, China*

(Dated: November 21, 2025)

GUTs unify quarks and leptons into same representations and predict correlations between their masses and mixing. We take new data of JUNO and perform numerical scans to explore the flavor space compatible with data in $SO(10)$ GUTs. The quark-lepton correlation shows the preference of normal ordering for light neutrino masses, predicts favored region of the CP-violating phase in neutrino oscillations, and classifies GUT models based their testability in neutrinoless double beta decay experiments. The quark-lepton correlation predicts mass spectrum of right-handed neutrinos, pointing to the energy scale of baryon and lepton number violation and providing sources for baryogenesis. We emphasize that, as the high precision measurements of neutrino physics is coming, the quark-lepton correlation will provide increasingly important role in the testability of GUTs, complementary to the proton decay measurement.

PACS numbers:

I. INTRODUCTION

Grand Unified Theories (GUTs) do not just unify three gauge interactions of the Standard Model (SM), but also unify Yukawa interactions of quarks and leptons. Of particular interests are the $SO(10)$ GUTs [1] where all SM matter fields are arranged in 16-plets of $SO(10)$ and, as a consequence, all fermion masses and mixing are correlated [2–4]. While proton decays provides a smoking gun signature of GUTs [5–11], the quark-lepton correlation of masses and mixing might verify the unification in the Yukawa sector. Furthermore, as right-handed neutrinos (RHNs) are embedded into 16-plets, their mass spectrum and Yukawa couplings are predicted by the quark-lepton correlation, and successful leptogenesis become testable in the seesaw framework.

The historical intertwining between neutrino measurements and GUTs dates back to the early 1980's, when the first generation experiments represented by IMB and KamiokaNDE were operated (see in review [12]). Current best limits on proton decay is set by the second generation singularly comprised of Super-Kamiokande [13, 14]. The latter is most famous for its observation of atmospheric neutrino oscillation in 1998 [15].

JUNO [16], Hyper-K [17] and DUNE [18] are three main large-scale neutrino oscillation measurements in this stage. They will continue on proton decay measurements to test GUTs by pushing the sensitivities of one order of magnitude. In the meantime, the most important goals are the determination of the neutrino mass hierarchy (normal $m_1 < m_2 < m_3$ or inverted $m_3 < m_1 < m_2$) and measurement of the Dirac-type CP-violating phase δ . The octant of θ_{23} (1st octant $0 < \theta_{23} < 45^\circ$) and (2nd octant $45^\circ < \theta_{23} < 90^\circ$) will be confirmed and measurements of other oscillation parameters with precision up to sub-percent level will be performed.

JUNO released the first data on the measurement of $\sin^2 \theta_{12}$ and Δm_{21}^2 after two months of running, with pre-

cision improved by a factor of 1.6 relative to the combination of all previous measurements [19]. In the stage of high-precision neutrino data, the quark-lepton correlation provides tool of increasing significance to test GUTs complementary to proton decay. We will use the quark-lepton correlation in $SO(10)$ GUTs as a criteria to explore the preferred distribution of unresolved physical observables, including neutrino mass ordering, the favored range of the Dirac CP-violating phase, and effective mass in neutrinoless double beta decay. These quantities will all be tested in the precision era of neutrino physics. In addition, the quark-lepton correlation predicts right-handed neutrino mass spectrum, which touches to $B - L$ breaking scale and provides sources for baryon-antibaryon asymmetry in the observed Universe. The rest of this paper is organized as follows. Section II gives an overview on Yukawa couplings in $SO(10)$ GUTs. Numerical analysis based on quark-lepton correlation is performed in Section III. We summarise and discuss our results in Section IV.

II. OVERVIEW ON YUKAWAS

In $SO(10)$ GUTs, all matter fields, including SM fermions (quarks, charged leptons and the left-handed neutrinos) and right-handed neutrinos, of the same generation are arranged into a single 16-dim chiral representation 16_F . Following the decomposition $16 \times 16 = 10 + 120 + 126$, a “full” Higgs content for Yukawa couplings could be 10_H , 120_H and $\overline{126}_H$. Yukawa interactions in $SO(10)$ GUTs are generically given by

$$16_F [Y_{10} 10_H + Y_{126} \overline{126}_H + Y_{120} 120_H] 16_F + \text{h.c.} \quad (1)$$

Here, 10_H , 120_H can be either real or complex, which will be denoted with subscripts \mathbb{R} and \mathbb{C} , respectively, and $\overline{126}_H$ is always complex following their representation properties. Complexifying the Higgs induces couplings with the conjugates $(10_H^{\mathbb{C}})^*$ and $(120_H^{\mathbb{C}})^*$. They can be

forbidden by imposing the Peccei-Quinn (PQ) symmetry $U(1)_{PQ}$ [20, 21], which gives a compelling explanation of the strong CP problem [22]. The PQ symmetry is a global $U(1)$ symmetry in which fermions and Higgses transform as

$$\begin{aligned} 16_F &\rightarrow e^{i\alpha} 16_F, & 10_H^C &\rightarrow e^{-2i\alpha} 10_H^C, \\ \overline{126}_H^C &\rightarrow e^{-2i\alpha} \overline{126}_H^C, & 120_H^C &\rightarrow e^{-2i\alpha} 120_H^C. \end{aligned} \quad (2)$$

Accounting for 3 flavors of fermions, all Yukawa couplings are 3×3 matrices, and in particular, Y_{10} , Y_{126} are symmetric and Y_{120} is anti-symmetric in the flavor basis.

Following the symmetry breaking from GUTs to the SM, these Higgses are eventually decomposed to eight electroweak doublets in total,

$$h_i = \{\tilde{h}_{10}^u, h_{10}^d, \tilde{h}_{126}^u, h_{126}^d, \tilde{h}_{120_1}^u, h_{120_1}^d, \tilde{h}_{120_{15}}^u, h_{120_{15}}^d\}, \quad (3)$$

where $\tilde{h}_{10}^u = i\sigma_2(h_{10}^u)^*$ [23]. These field decompositions introduce particles beyond the SM spectrum and the SM higgs is regarded as the lightest and massless one of their eigenstates. Below the GUT scale, it is convenient to write out Yukawa coupling matrices for quarks and leptons

$$\begin{aligned} Y_u &= c_{10}^u Y_{10} + c_{126}^u Y_{126} + (c_{120_1}^u + c_{120_{15}}^u) Y_{120}, \\ Y_d &= c_{10}^d Y_{10} + c_{126}^d Y_{126} + (c_{120_1}^d + c_{120_{15}}^d) Y_{120}, \\ Y_e &= c_{10}^d Y_{10} - 3c_{126}^d Y_{126} + (c_{120_1}^d - 3c_{120_{15}}^d) Y_{120}, \\ Y_\nu &= c_{10}^u Y_{10} - 3c_{126}^u Y_{126} + (c_{120_1}^u - 3c_{120_{15}}^u) Y_{120}. \end{aligned} \quad (4)$$

And mass matrices for quarks and leptons as well as the Dirac mass matrix for neutrinos are generated after the electroweak symmetry breaking, $M_f = Y_f v$ with $f = u, d, e, \nu$ and $v = 174$ GeV. The $\overline{126}_H$ Higgs contains scalars of the charge $B - L = 2$. They are essential to generate light neutrino masses via seesaw mechanism,

$$\begin{aligned} M_R &= v_S Y_{126}, \\ M_\nu &= -Y_\nu M_R^{-1} Y_\nu^T v^2, \end{aligned} \quad (5)$$

where v_S is the scalar VEV and we have assumed type-I seesaw dominance. Since all SM fermion mass matrices M_u, M_d, M_e and M_ν are correlated, it is obvious that masses of quarks and leptons, and the consequent flavor mixing (i.e., Cabibbo-Kobayashi-Maskawa (CKM) and Pontecorvo-Maki-Nakagawa-Sakata (PMNS) mixing), are all correlated via the above formulas.

While the general Yukawa couplings in Eq. (1) leaves plenty room to fit data of fermion masses and mixing, economical models have been considered to reduce the number of free parameters. We discuss the economical and realistic Higgs content to be included in this work. First, one single Higgs multiplet (either 10_H , $\overline{126}_H$ or 120_H) is not enough since the prediction of generate fermion masses and no flavor mixing in either quark and lepton sector. To explain tiny masses for light neutrinos, $\overline{126}_H$ must be included since it is the only Higgs

TABLE I: A complete list of possible combinations of Higgs content in renormalizable $SO(10)$ GUTs with all fermions arranged in 16_F .

Higgs content	Whether realistic in fitting fermion data
Only one Higgs	No, no flavor mixing
$10_H^{\mathbb{R},C}, 120_H^{\mathbb{R},C}$	No, massless light neutrinos
$10_H^{\mathbb{R}}, \overline{126}_H^C$	No, small hierarchy between m_b and m_t
$120_H^{\mathbb{R},C}, \overline{126}_H^C$	No, inconsistent with mixing data
$10_H^C, \overline{126}_H^C$	Yes, imposing $U(1)_{PQ}$ leads to M1
$10_H^{\mathbb{R}}, \overline{126}_H^C, 120_H^{\mathbb{R}}$	Yes, assuming SCPV leads to M2
$10_H^C, \overline{126}_H^C, 120_H^C$	Yes, imposing $U(1)_{PQ} \times Z_2^P$ leads to M3

TABLE II: Representative models to be used in fitting fermion data, their main features and number of free parameters.

Model	Main features	n_{para}
M1	Only Y_{10}, Y_{126}	19
M2	Real Y_{10}, Y_{126}, Y_{120}	19
M3	Hermitian Y_u, Y_d, Y_e, Y_ν	18

involving a SM singlet with charge $B - L = 2$, which is necessary to generate Majorana masses for neutrinos via seesaw mechanisms. The minimal extension is by adding a real $10_H^{\mathbb{R}}$ into the theory. However, it cannot explain the large hierarchy between m_b and m_t [21]. On the other hand, the model with $(\overline{126}_H, 120_H)$ is found to be unable to fit all the fermion masses and mixing angles in the three generation case [24, 25]. Then, we are left with a few realistic choices in fitting data, either the minimal Higgs content $(10_H^C, \overline{126}_H^C)$ or a complete list $(10_H, \overline{126}_H, 120_H)$. Among them, we will focus on three compelling models.

- M1 – $(10_H^C, \overline{126}_H^C)$ with $U(1)_{PQ}$. This one introduces the minimal Higgs contents among the realistic models [20]. Imposing $U(1)_{PQ}$ forbid terms with $(10_H^C)^*$ and thus only Y_{10} and Y_{126} are present [26–29]. Without loss of generality, we rotate the flavor basis to keep Y_{126} always real and diagonal. There are $6 \times 2 + 3$ real parameters in Y_{10} and Y_{126} . Additional free parameters includes the relative size and phases among $c_{10,126}^{u,d}$. In total, we have 19 free parameters in the Yukawa sector.
- M2 – $(10_H^{\mathbb{R}}, \overline{126}_H^C, 120_H^{\mathbb{R}})$ with SCPV. Complex Yukawas Y_{10}, Y_{126} and Y_{120} leave enough room to fit data. Imposing CP symmetry at high scale reduces the number of free parameters [30–33]. In the basis of diagonal Y_{126} , there are $6 + 3 + 3$ real parameters in Y_{10}, Y_{126}, Y_{120} . The Higgses gain complex VEVs and induce spontaneous CP violation (SCPV). This model introduce also

19 free parameters in the Yukawa sector competitive to M1.

- M3 – $(10_H^C, \overline{126}_H^C, 120_H^C)$ with $U(1)_{PQ} \times Z_2^P$. This model includes a full list of Higgs multiplets [23–25]. $U(1)_{PQ}$ forbids couplings to the complex conjugate of 10_H^C or 120_H^C . Z_2^P represents the left-right parity symmetry $\psi_L \leftrightarrow \psi_R$, which results in Hermitian Yukawa matrices Y_u, Y_d, Y_e, Y_ν [34]. This symmetry is achieved via a CP parity symmetry at high scale, to guarantee real Y_{10}, Y_{126} and Y_{120} . Combining the CP parity with the internal matter parity, i.e., the D parity [35], $\psi_L \leftrightarrow \psi_R^C$, of $SO(10)$ gives rise to Z_2^P . A maximal CP violation is achieved spontaneously if the VEV of 120_H^C is orthogonal to the other two Higgs VEVs in the complex plane, but Z_2^P is left unbroken [36].

We refer to Appendix A for detailed parameterizations of these models.

III. NUMERICAL ANALYSIS

We explore the parameter space allowed by current experiments and discuss their physical predictions for the above three models. The χ^2 function is defined as

$$\chi^2 = \sum_{i=1}^{n_{\text{obs}}} \left(\frac{\mathcal{O}_i - \mathcal{O}_i^{\text{bf}}}{\sigma_{\mathcal{O}_i}} \right)^2, \quad (6)$$

where \mathcal{O}_i is the i -th theoretical prediction, and $\mathcal{O}_i^{\text{bf}}$ is the corresponding i -th experimental best-fit (bf) value, and the $\sigma_{\mathcal{O}_i}$ is the 1σ uncertainty. We take $n_{\text{obs}} = 18$ observables into fitting, including 9 charged fermion masses, 3 angles and 1 phase in the CKM mixing matrix, 2 mass-squared differences and 3 angles in the PMNS mixing matrix. All data are listed in Appendix A. In the neutrino sector, we take NuFIT 6.0 [37] but replace data of Δm_{21}^2 and $\sin^2 \theta_{12}$ (best-fits $\pm 1\sigma$) with the most recent JUNO data,

$$\begin{aligned} \Delta m_{21}^2 &= (7.50 \pm 0.12) \times 10^{-5} \text{eV}^2, \\ \sin^2 \theta_{12}^l &= 0.3092 \pm 0.0087, \end{aligned} \quad (7)$$

It is worth noting that NuFIT with SK atmospheric data prefers θ_{23} in the first octant ($\theta_{23} < 45^\circ$) and that without SK atmospheric data prefers the second octant ($\theta_{23} > 45^\circ$). We have taken both data into account to check the preference of the θ_{23} octant in those GUT models. The up-to-date experimental constraint on the Dirac CP-violating phase δ is still weak, and thus is not included in the χ^2 . Instead, we treat δ as a prediction of the model, together with other predictions including the effective masses appearing in β decay m_β , neutrinoless double- β decay $m_{\beta\beta}$, neutrino mass sum contributing in cosmology $\sum m_i$, and right-handed neutrino mass spectrum M_1, M_2, M_3 .

We first comment on the preference of neutrino mass ordering in $SO(10)$ GUTs. We have done scan in both

normal ordering (NO) and inverted ordering (IO) with the same computation power. In MI with the IO, M1 cannot minimize χ^2/n_{obs} below 280; In M2 and M3, we have found points marginally consistent with data with $\chi^2/n_{\text{obs}} = 35$ and $\chi^2/n_{\text{obs}} = 19$ respectively in the IO. In general, scanning for IO is more difficult than the NO case. In all three models, NO is highly favored by the quark-lepton correlation.

In the NO, general results are shown in Fig. 1, with benchmarks presented in Appendix B. We summarize the results below.

- By taking data of θ_{23} in both octants, we find a slight preference on the 1st octant in M2, but no significant preference of the octant in M1 and M3.
- Distributions of δ are different in three models. δ is restricted in the region $[-90^\circ, +90^\circ]$ in M2, preferred in the same region in M3, and nearly flatly distributed in the whole parameter space in M1.
- m_1 is predicted around in the region $[0.002, 0.01]$ eV in M1, $m_1 \lesssim 0.001$ eV in M2 and is mainly distributed in $[10^{-4}, 10^{-2}]$ eV in M3.
- $m_{\beta\beta}$ in M1 is predicted in a narrow regime $[0.004, 0.01]$ eV, which can be tested in the future $0\nu 2\beta$ experiments. Values of $m_{\beta\beta}$ in M1 is smaller, in the region $[0.002, 0.004]$ eV, below the experimental sensitivity. The predicted region in M3 overlaps with both models.

We discuss the predictions of RHN mass spectrum and potentially consequent phenomenon. These models are predicted very different mass spectrums for RHNs. We have confirmed the large hierarchy of RHN masses in M2 which has been studied in [32], where the lightest one can be as small as 10^4 GeV and the heaviest one can reach 10^{15} GeV. However, more points show the lightest mass M_1 located in the interval $[10^6, 3 \cdot 10^7]$ GeV. This regime has not been discovered before. Both M1 and M3 shows much smaller hierarchies. M1 gives a clear prediction on M_1 around $[10^9, 10^{10}]$ GeV and the highest one $M_3 \sim [10^{12}, 10^{13}]$ GeV. where most points give $M_1/M_3 \sim 10^{-3}$. Predictions in M3 are more diverse, although a lot of them gives $M_1 \sim 10^{10}$ GeV and $M_3 \sim 10^{13}$ GeV. This result is consistent with former results [23], but we have found more parameter space.

We further comment that a clear prediction of RHN mass spectrum serves as the basis for numerous interesting research avenues. We briefly address them below. RHNs provide an explanation of baryon-antibaryon asymmetry via the mechanism of leptogenesis. This is quantitatively calculated via the quark-lepton correlation in $SO(10)$ GUTs. A successful thermal leptogenesis requires M_1 heavier than 10^9 GeV [38], which applies for most points in M1 and M3. However, this condition is satisfied in M2, and inspired alternative scenario, e.g., N_2 leptogenesis [39] might succeed in some parameter space [33]. In a perturbative theory, all RHN masses should not

be heavier than the $B - L$ energy scale. That means this scale should be heavier than $M_3 \sim 10^{13}$ GeV for most points in M1 and M3. In M2, the heaviest RHN can be as heavy as 10^{15} GeV. A $B - L$ scale above this value requires special RG effects to be included in the gauge unification.

IV. CONCLUSION AND DISCUSSIONS

GUTs unify quarks and leptons and predict correlation between their masses and mixing. We emphasize that the quark-lepton correlation can play increasingly important role to test GUTs with the help of high-precision neutrino measurements in the coming decade.

We begin with a brief review on the fermion masses and mixing in SO(10) GUTs. Then we take three representative GUT models as examples to explore the flavor space consistent with experimental data. In particular, the most recent JUNO data has been taken into account. The quark-lepton correlation shows the preferred distribution of unresolved physical observables. We argue that inverted ordering for neutrino masses are disfavored in

A. Details of fitting procedure

Regarding VEVs of Higgs doublets in $10_H, \overline{126}_H, 120_H$, without loss of generality, v_{126}^u can be taken to be real, and remaining VEVs are generally complex. Moreover, SM singlet S VEV v_S can also be real, concretely we write

$$\begin{aligned} c_{10}^u &= |c_{10}^u|e^{i\alpha}, \quad c_{10}^d = |c_{10}^d|e^{i\beta}, \\ c_{126}^u &= |c_{126}^u|, \quad c_{126}^d = |c_{126}^d|e^{i\omega}, \quad v_S = |v_S|, \\ c_{120_1}^u + c_{120_{15}}^u &= |c_{120_1}^u + c_{120_{15}}^u|e^{i\lambda}, \\ c_{120_1}^d + c_{120_{15}}^d &= |c_{120_1}^d + c_{120_{15}}^d|e^{i\rho}, \\ c_{120_1}^u - 3c_{120_{15}}^u &= |c_{120_1}^u - 3c_{120_{15}}^u|e^{i\gamma}, \\ c_{120_1}^d - 3c_{120_{15}}^d &= |c_{120_1}^d - 3c_{120_{15}}^d|e^{i\eta}, \end{aligned} \quad (\text{A1})$$

where these coefficients were obtained from VEVs

$$\begin{aligned} &\{\langle h_{10}^u \rangle, \langle h_{10}^d \rangle, \langle h_{126}^u \rangle, \langle h_{126}^d \rangle, \\ &\langle h_{120_1}^u \rangle, \langle h_{120_{15}}^u \rangle, \langle h_{120_1}^d \rangle, \langle h_{120_{15}}^d \rangle\} \\ &= \{c_{10}^u, c_{10}^d, c_{126}^u, c_{126}^d, \\ &c_{120_1}^u, c_{120_1}^d, c_{120_{15}}^u, c_{120_{15}}^d\} \times v_{\text{EW}}. \end{aligned} \quad (\text{A2})$$

Furthermore, we define the following Yukawa matrices and real parameters

$$\begin{aligned} D &= |c_{126}^u|Y_{126}, \quad S = |c_{10}^u|Y_{10}, \quad A = |c_{120_1}^u + c_{120_{15}}^u|Y_{120}, \\ v_R &= \frac{|v_S|}{|c_{126}^u|}, \quad r_1 = \frac{|c_{126}^d|}{|c_{126}^u|}, \quad r_2 = \frac{|c_{10}^d|}{|c_{10}^u|}, \quad r_3 = \frac{|c_{120_1}^d + c_{120_{15}}^d|}{|c_{120_1}^u + c_{120_{15}}^u|}, \\ r_4 &= \frac{|c_{120_1}^d - 3c_{120_{15}}^d|}{|c_{120_1}^u + c_{120_{15}}^u|}, \quad r_5 = \frac{|c_{120_1}^u - 3c_{120_{15}}^u|}{|c_{120_1}^u + c_{120_{15}}^u|}. \end{aligned} \quad (\text{A3})$$

With the above preparation, three models in this paper can be reparameterized, which are shown below.

SO(10) GUTs. The Dirac CP-violating phase and neutrinoless double beta decay are predicted differently in these models. Forthcoming measurements will be able to classify GUT models. These quantities will all be tested in the precision era of neutrino physics. The quark-lepton correlation further predicts right-handed neutrino masses. Different hierarchies of their mass scales point to different scenarios of leptogenesis in explanation of matter-antimatter asymmetry in our observed universe. The restrictions on the $B - L$ scale touches to the gauge unification in GUTs. We suggest to use the quark-lepton correlation as a tool to evaluate GUTs in the precision era of neutrino physics.

Acknowledgments

This work was supported by the National Natural Science Foundation of China (NSFC) under Grant Nos. 12205064, 12347103, and Zhejiang Provincial Natural Science Foundation of China under Grant No. LDQ24A050002.

M1, $10_H^{\text{C}} + \overline{126}_H^{\text{C}}$ with $U(1)_{\text{PQ}}$

$$\begin{aligned} Y_u &= S + D, \\ Y_d &= r_2 S + e^{i\omega} r_1 D, \\ Y_e &= r_2 S - 3e^{i\omega} r_1 D, \\ Y_\nu &= S - 3D, \\ M_R &= v_R D, \end{aligned} \quad (\text{A4})$$

where the phase of c_{10}^u , can be absorbed into S and an overall phase between S terms and D terms in Y_d is unphysical and has been ignored. Here we follow the convention in Ref. [40], with a basis where the symmetric matrix D is real and diagonal, whence S becomes a general complex symmetric matrix. r_1, r_2, v_R are real parameters and ω is a phase.

M2, $10_H^{\text{R}} + \overline{126}_H^{\text{C}} + 120_H^{\text{R}}$ with SCPV

As $10_H, 120_H$ are real fields, VEVs of Higgs doublets in these two fields have relations $v_{10}^d = v_{10}^{u*}, v_{120_1}^d + v_{120_{15}}^d = v_{120_1}^{u*} + v_{120_{15}}^{u*}, v_{120_1}^d - 3v_{120_{15}}^d = v_{120_1}^{u*} - 3v_{120_{15}}^{u*}$. Next, we follow the convention in Ref. [33], the Dirac mass matrices of fermions can be reparameterized as

$$\begin{aligned} Y_u &= e^{i\alpha} S + D + e^{i\lambda} A, \\ Y_d &= e^{-i\alpha} S + e^{i\omega} r_1 D + e^{-i\lambda} A, \\ Y_e &= e^{-i\alpha} S - 3e^{i\omega} r_1 D + e^{-i\gamma} r_4 A, \\ Y_\nu &= e^{i\alpha} S - 3D + e^{i\gamma} r_4 A, \\ M_R &= v_R D. \end{aligned} \quad (\text{A5})$$

Due to CP invariance, Y_{10}, Y_{126}, Y_{120} are all real matrices, equivalently S, D, A are real matrices and

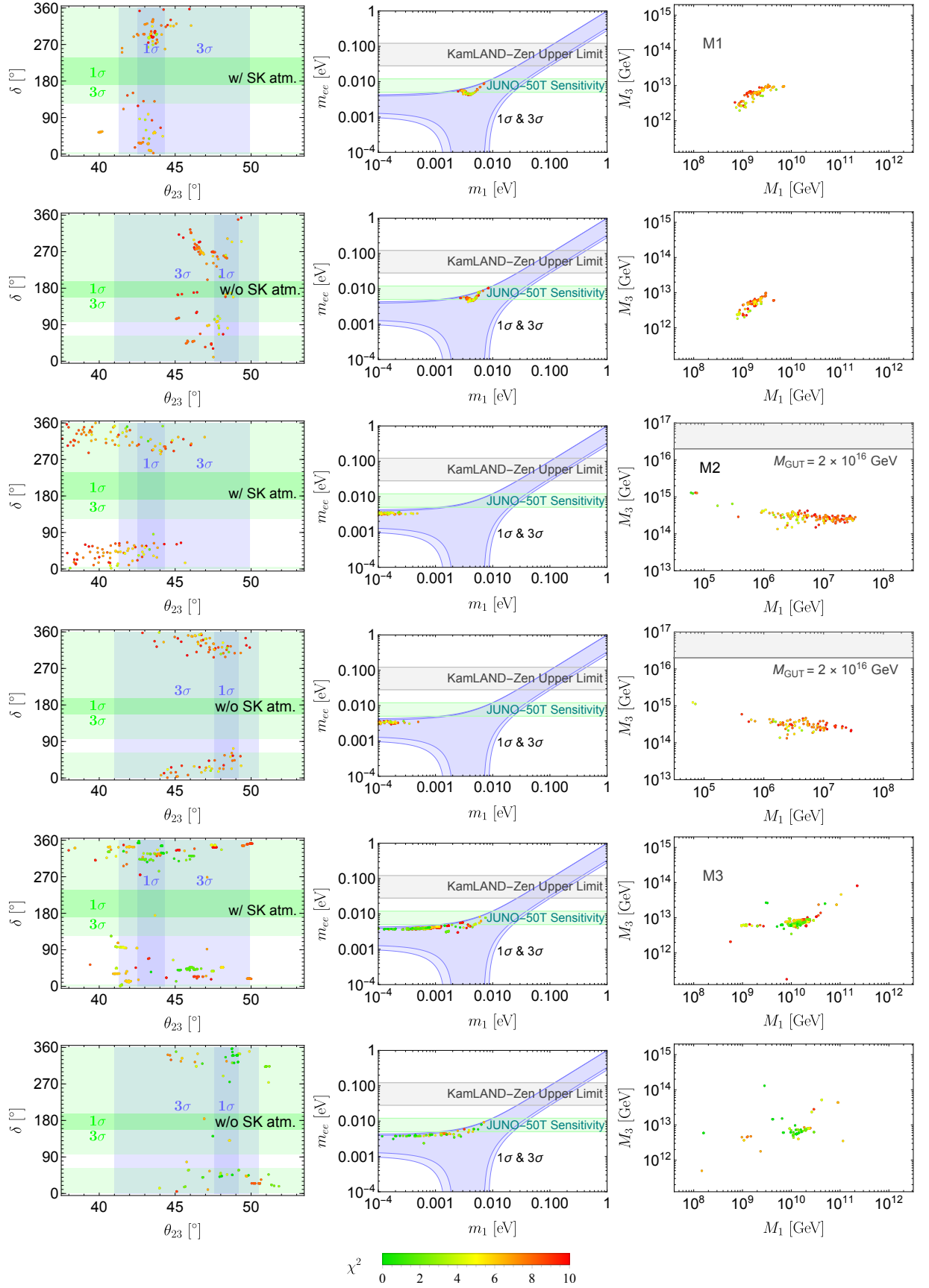


FIG. 1: Predictions of GUT models M1, M2 and M3.

M_R is a real symmetric matrix. Here, we work in a basis where Y_{126} is diagonal and positive, resulting D is diagonal and positive. S is real symmetric and A is real antisymmetric. r_1, r_4, v_R are real parameters and $\alpha, \lambda, \gamma, \omega$ are phases.

M3, $10_H^C + \overline{126}_H^C + 120_H^C$ with $U(1)_{PQ} \times Z_2^P$

The Dirac mass matrices of fermions are reparameterized as

$$\begin{aligned} Y_u &= S + D + iA, \\ Y_d &= r_2 S + r_1 D + ir_3 A, \\ Y_e &= r_2 S - 3r_1 D + ir_4 A, \\ Y_\nu &= S - 3D + ir_5 A, \\ M_R &= v_R D. \end{aligned} \quad (A6)$$

Here, we follow the convention in Ref. [23], as CP invariance above the GUT scale and spontaneous CP violation (SCPV) below the GUT scale, S, D, A are real matrices, resulting Y_u, Y_d, Y_e, Y_ν are Hermitian matrices and M_R is a real symmetric matrix. Consistent with previous models, we still choose a basis where D is diagonal and positive, S is real symmetric and A is real antisymmetric. $r_1, r_2, r_3, r_4, r_5, v_R$ are real parameters.

Parameters of these models are summarized in Table III.

Data (best-fits $\pm 1\sigma$) for quark Yukawas and mixing parameters, as well as charged lepton Yukawas, are listed below, taken from [30] with RG effect running up to $M_{\text{GUT}} = 2 \times 10^{16}$ GeV.

$$\begin{aligned} y_u &= (2.54 \pm 0.86) \cdot 10^{-6}, & y_d &= (6.56 \pm 0.65) \cdot 10^{-6}, \\ y_c &= (1.37 \pm 0.04) \cdot 10^{-3}, & y_s &= (1.24 \pm 0.06) \cdot 10^{-4}, \\ y_t &= (0.428 \pm 0.003), & y_b &= (5.7 \pm 0.005) \cdot 10^{-3}, \\ \theta_{12}^q &= (0.227 \pm 0.0006), & \theta_{13}^q &= (4.202 \pm 0.13) \cdot 10^{-3}, \\ \theta_{23}^q &= (4.858 \pm 0.06) \cdot 10^{-2}, & \delta^q &= (1.207 \pm 0.054); \end{aligned} \quad (A7)$$

$$\begin{aligned} y_e &= (2.703 \pm 0.027) \cdot 10^{-6}, & y_\mu &= (5.707 \pm 0.057) \cdot 10^{-4}, \\ y_\tau &= (9.702 \pm 0.0097) \cdot 10^{-3}, \end{aligned} \quad (A8)$$

For charged lepton yukawas, we have quoted error to be 1% uncertainty in their masses to relax the difficulty induced by the tiny experimental errors of charged lepton masses [32]. Oscillation data except Δm_{21}^2 and $\sin^2 \theta_{12}$ in the normal ordering are taken from NuFIT 6.0 [37]. In the normal ordering,

$$\begin{aligned} \sin^2 \theta_{23} &= 0.561 \pm 0.014, & \sin^2 \theta_{13} &= 0.02195 \pm 0.00056, \\ \Delta m_{31}^2 &= (2.534 \pm 0.024) \times 10^{-3} \text{eV}^2, \end{aligned} \quad (A9)$$

for IC19 without SK atmospheric data and

$$\sin^2 \theta_{23} = 0.470 \pm 0.015, \quad \sin^2 \theta_{13} = 0.02215 \pm 0.00057$$

$$\Delta m_{31}^2 = (2.513 \pm 0.020) \times 10^{-3} \text{eV}^2, \quad (A10)$$

for IC24 with SK atmospheric data. In the inverted ordering, those without or with SK atmospheric data are respectively given by

$$\begin{aligned} \sin^2 \theta_{23} &= 0.562 \pm 0.014, & \sin^2 \theta_{13} &= 0.02224 \pm 0.00057 \\ \Delta m_{32}^2 &= (-2.510 \pm 0.025) \times 10^{-3} \text{eV}^2, \end{aligned} \quad (A11)$$

$$\begin{aligned} \sin^2 \theta_{23} &= 0.550 \pm 0.014, & \sin^2 \theta_{13} &= 0.02231 \pm 0.00057 \\ \Delta m_{32}^2 &= (-2.484 \pm 0.020) \times 10^{-3} \text{eV}^2. \end{aligned} \quad (A12)$$

NuFIT data of $\sin^2 \theta_{12}$ and Δm_{21}^2 in the inverted ordering keep the same,

$$\begin{aligned} \sin^2 \theta_{12} &= 0.308 \pm 0.012, \\ \Delta m_{21}^2 &= (7.49 \pm 0.19) \times 10^{-5} \text{eV}^2, \end{aligned} \quad (A13)$$

The scan procedure is performed as below.

1. We begin with 25000 random points whose parameters x_i^0 (i runs through free parameters of every models) are within their defined region shown in Tab. III, from which we obtain Dirac mass matrices, and the light neutrino mass matrix are obtained through type-I dominant seesaw. The initial value of χ^2 is usually very large, reaching the order of 10^8 .
2. We further minimize χ^2 by varying parameters of initial points x_i^0 within the range of $x_i^0(1 \pm \varepsilon)$. Here, ε describes the degree to which the size of the interval parameters x_i^0 can vary in. Furthermore, ε can be adaptively adjusted by code within the range of $(10^{-4}, 0.03)$ to achieve smaller χ^2 . Then, we find a series of points with smaller χ^2 , whose parameters are denoted as x_i^1 .
3. We repeat step 2 by replacing x_i^{k+1} with x_i^k and minimize χ^2 . We run the iteration number k up to 2×10^6 . Finally, we select points with $\chi^2/n_{\text{obs}} \leq 10$.

Our scan is performed on the HIAS cluster with 3000 CPU cores available. Model M1 with normal ordering and θ_{23} in 1st octant (M1N1) or M1 with normal ordering and θ_{23} in 2nd octant (M1N2) complete their scan using 2048 CPU cores in 16 hours and get final $\chi^2/n_{\text{obs}} = 3.87, 3.10$. Model M2 with normal ordering and θ_{23} in 1st octant (M2N1) or M2 with normal ordering and θ_{23} in 2nd octant (M2N2) complete their scan using 896 CPU cores in 12 hours and get final $\chi^2/n_{\text{obs}} = 1.34, 2.65$. Model M3 with normal ordering and θ_{23} in 1st octant (M3N1) or M3 with normal ordering and θ_{23} in 2nd octant (M3N2) complete their scan using 1000 CPU cores in 16 hours and get final $\chi^2/n_{\text{obs}} = 0.27, 0.04$. Model M1 with inverted ordering and θ_{23} in 1st octant (M1I1) or M1 with inverted ordering and θ_{23} in 2nd octant (M1I2) complete their scan using 768 CPU cores in 9 hours and get final $\chi^2/n_{\text{obs}} = 280.18, 280.05$. Model M2 with inverted ordering and θ_{23} in 1st octant (M2I1) or M2 with

TABLE III: Parameters counting for 3 different models.

Label	Free parameters
M1 ($n_{\text{para}} = 19$)	$\{r_1, r_2\} \in (-10, 10)$, $m_0 \in (0, 1)$ eV, $\omega \in [0, 2\pi)$, $D : \{D_{11}, D_{22}, D_{33}\} \in (0, 1)$, $S : \{S_{11}e^{is_1}, S_{12}e^{is_2}, S_{13}e^{is_3}, S_{22}e^{is_4}, S_{23}e^{is_5}, S_{33}e^{is_6}\} \in (-10, 10)e^{i[0, 2\pi)}$
M2 ($n_{\text{para}} = 19$)	$\{r_1, r_4\} \in (-10, 10)$, $m_0 \in (0, 1)$ eV, $\{\alpha, \lambda, \gamma, \omega\} \in [0, 2\pi)$, $D : \{D_{11}, D_{22}, D_{33}\} \in (0, 1)$, $S : \{S_{11}, S_{12}, S_{13}, S_{22}, S_{23}, S_{33}\} \in (-10, 10)$, $A : \{A_{12}, A_{13}, A_{23}\} \in (-10, 10)$
M3 ($n_{\text{para}} = 18$)	$\{r_1, r_2, r_3, r_4, r_5\} \in (-10, 10)$, $m_0 \in (0, 1)$ eV, $D : \{D_{11}, D_{22}, D_{33}\} \in (0, 1)$, $S : \{S_{11}, S_{12}, S_{13}, S_{22}, S_{23}, S_{33}\} \in (-10, 10)$, $A : \{A_{12}, A_{13}, A_{23}\} \in (-10, 10)$

TABLE IV: Benchmark fit values and predictions in 3 models. Each benchmark is named, e.g., BM1N1: Benchmark of M1 with Normal ordering and 1st octant of θ_{23} .

Physical Quantity	M1		M2		M3	
	BM1N1	BM1N2	BM2N1	BM2N2	BM3N1	BM3N2
$y_u/10^{-6}$	4.1841	4.08227	2.81639	7.43413	2.57195	2.51847
$y_c/10^{-3}$	1.40605	1.37123	1.36956	1.38067	1.35808	1.36456
y_t	0.428387	0.42744	0.428109	0.427893	0.428165	0.427999
$y_d/10^{-6}$	1.90741	2.33024	3.81711	6.40586	7.63478	6.50436
$y_s/10^{-4}$	1.20008	1.35263	1.17849	1.35147	1.22573	1.22668
$y_b/10^{-2}$	0.56536	0.572574	0.569053	0.569561	0.569812	0.571195
$y_e/10^{-6}$	2.70615	2.70217	2.70694	2.70512	2.7012	2.70299
$y_\mu/10^{-4}$	5.67557	5.64767	5.72306	5.68859	5.70761	5.70903
$y_\tau/10^{-2}$	0.979853	0.971086	0.968229	0.969382	0.968972	0.968018
θ_{12}^q	0.227388	0.227475	0.226987	0.227082	0.22744	0.227423
$\theta_{23}^q/10^{-2}$	4.78722	4.86052	4.8502	4.85534	4.86112	4.86603
$\theta_{13}^q/10^{-3}$	4.44527	4.36218	4.15777	4.03305	4.19948	4.19105
δ^q	1.10098	1.20818	1.17491	1.15692	1.25108	1.23699
$\Delta m_{21}^2/10^{-5}$ [eV]	7.49642	7.51729	7.48813	7.3983	7.4778	7.49186
$\Delta m_{31}^2/10^{-3}$ [eV]	2.51096	2.53253	2.51289	2.53819	2.51446	2.53476
$\sin^2\theta_{12}^l$	0.306389	0.315291	0.299572	0.28436	0.306322	0.307802
$\sin^2\theta_{23}^l$	0.469948	0.551379	0.444945	0.561499	0.484914	0.566208
$\sin^2\theta_{13}^l$	0.021243	0.0210321	0.0223411	0.0223394	0.0219516	0.0218592
$\chi^2/(n_{\text{obs}} = 18)$	3.87235	3.09649	1.33774	2.64746	0.267685	0.0398901
m_1 [eV]	0.00428924	0.00580787	0.0000445112	0.000277348	0.000786665	0.000344881
m_β [eV]	0.0985221	0.102458	0.0939997	0.09378	0.0940432	0.0940024
$m_{\beta\beta}$ [eV]	0.0672365	0.0872486	0.0604685	0.0602027	0.0644098	0.0625105
δ [°]	285.682	208.427	350.862	310.236	346.342	339.851
M_1 [GeV]	1.15×10^9	1.43×10^9	60633.6	2.56×10^6	6.56×10^9	1.26×10^{10}
M_2 [GeV]	1.74×10^{11}	1.72×10^{11}	4.28×10^{12}	7.44×10^{11}	1.37×10^{11}	2.28×10^{11}
M_3 [GeV]	3.11×10^{12}	3.05×10^{12}	1.29×10^{15}	2.15×10^{14}	6.26×10^{12}	5.52×10^{12}

inverted ordering and θ_{23} in 2nd octant (M2I2) complete their scan using 768 CPU cores in 9 hours and get final $\chi^2/n_{\text{obs}} = 34.47, 44.98$. Model M3 with inverted ordering and θ_{23} in 1st octant (M3I1) or M3 with in-

verted ordering and θ_{23} in 2nd octant (M3I2) complete their scan using 768 CPU cores in 9 hours and get final $\chi^2/n_{\text{obs}} = 19.14, 19.04$.

B. Benchmark studies

We show a few benchmark points in M1, M2 and M3 extracted from the scan in Tab. IV.

- [1] H. Fritzsch and P. Minkowski, *Annals Phys.* **93**, 193-266 (1975) doi:10.1016/0003-4916(75)90211-0
- [2] M. S. Chanowitz, J. R. Ellis and M. K. Gaillard, *Nucl. Phys. B* **128**, 506-536 (1977) doi:10.1016/0550-3213(77)90057-8
- [3] P. Ramond, [arXiv:hep-ph/9809459 [hep-ph]].
- [4] J. A. Harvey, D. B. Reiss and P. Ramond, *Nucl. Phys. B* **199**, 223-268 (1982) doi:10.1016/0550-3213(82)90346-7
- [5] S. Weinberg, *Phys. Rev. Lett.* **43**, 1566-1570 (1979) doi:10.1103/PhysRevLett.43.1566
- [6] F. Wilczek and A. Zee, *Phys. Rev. Lett.* **43**, 1571-1573 (1979) doi:10.1103/PhysRevLett.43.1571
- [7] S. Weinberg, *Phys. Rev. D* **22**, 1694 (1980) doi:10.1103/PhysRevD.22.1694
- [8] S. Weinberg, *Phys. Rev. D* **26**, 287 (1982) doi:10.1103/PhysRevD.26.287
- [9] N. Sakai and T. Yanagida, *Nucl. Phys. B* **197**, 533 (1982) doi:10.1016/0550-3213(82)90457-6
- [10] S. Dimopoulos, S. Raby and F. Wilczek, *Phys. Lett. B* **112**, 133 (1982) doi:10.1016/0370-2693(82)90313-6
- [11] J. R. Ellis, D. V. Nanopoulos and S. Rudaz, *Nucl. Phys. B* **202**, 43-62 (1982) doi:10.1016/0550-3213(82)90220-6
- [12] P. Langacker, *Phys. Rept.* **72**, 185 (1981) doi:10.1016/0370-1573(81)90059-4
- [13] K. Abe *et al.* [Super-Kamiokande], *Phys. Rev. D* **90**, no.7, 072005 (2014) doi:10.1103/PhysRevD.90.072005 [arXiv:1408.1195 [hep-ex]].
- [14] K. Abe *et al.* [Super-Kamiokande], *Phys. Rev. D* **95**, no.1, 012004 (2017) doi:10.1103/PhysRevD.95.012004 [arXiv:1610.03597 [hep-ex]].
- [15] Y. Fukuda *et al.* [Super-Kamiokande], *Phys. Rev. Lett.* **81**, 1562-1567 (1998) doi:10.1103/PhysRevLett.81.1562 [arXiv:hep-ex/9807003 [hep-ex]].
- [16] F. An *et al.* [JUNO], *J. Phys. G* **43**, no.3, 030401 (2016) doi:10.1088/0954-3899/43/3/030401 [arXiv:1507.05613 [physics.ins-det]].
- [17] R. Acciarri *et al.* [DUNE], [arXiv:1512.06148 [physics.ins-det]].
- [18] K. Abe *et al.* [Hyper-Kamiokande], [arXiv:1805.04163 [physics.ins-det]].
- [19] A. Abusleme *et al.* [JUNO], [arXiv:2511.14593 [hep-ex]].
- [20] K. S. Babu and R. N. Mohapatra, *Phys. Rev. Lett.* **70**, 2845-2848 (1993) doi:10.1103/PhysRevLett.70.2845 [arXiv:hep-ph/9209215 [hep-ph]].
- [21] B. Bajc, A. Melfo, G. Senjanovic and F. Vissani, *Phys. Rev. D* **73**, 055001 (2006) doi:10.1103/PhysRevD.73.055001 [arXiv:hep-ph/0510139 [hep-ph]].
- [22] R. D. Peccei and H. R. Quinn, *Phys. Rev. Lett.* **38**, 1440-1443 (1977) doi:10.1103/PhysRevLett.38.1440
- [23] B. Fu, S. F. King, L. Marsili, S. Pascoli, J. Turner and Y. L. Zhou, *JHEP* **11**, 072 (2022) doi:10.1007/JHEP11(2022)072 [arXiv:2209.00021 [hep-ph]].
- [24] A. S. Joshipura and K. M. Patel, *Phys. Rev. D* **83**, 095002 (2011) doi:10.1103/PhysRevD.83.095002 [arXiv:1102.5148 [hep-ph]].
- [25] A. Dueck and W. Rodejohann, *JHEP* **09**, 024 (2013) doi:10.1007/JHEP09(2013)024 [arXiv:1306.4468 [hep-ph]].
- [26] V. S. Mummidi and K. M. Patel, *JHEP* **12**, 042 (2021) doi:10.1007/JHEP12(2021)042 [arXiv:2109.04050 [hep-ph]].
- [27] T. Ohlsson and M. Pernow, *JHEP* **06**, 085 (2019) doi:10.1007/JHEP06(2019)085 [arXiv:1903.08241 [hep-ph]].
- [28] K. S. Babu and S. Khan, *Phys. Rev. D* **92**, no.7, 075018 (2015) doi:10.1103/PhysRevD.92.075018 [arXiv:1507.06712 [hep-ph]].
- [29] G. Altarelli and D. Meloni, *JHEP* **08**, 021 (2013) doi:10.1007/JHEP08(2013)021 [arXiv:1305.1001 [hep-ph]].
- [30] K. S. Babu, B. Bajc and S. Saad, *JHEP* **02**, 136 (2017) doi:10.1007/JHEP02(2017)136 [arXiv:1612.04329 [hep-ph]].
- [31] S. Saad, *JHEP* **04**, 058 (2023) doi:10.1007/JHEP04(2023)058 [arXiv:2212.05291 [hep-ph]].
- [32] K. S. Babu, P. Di Bari, C. S. Fong and S. Saad, *JHEP* **10**, 190 (2024) doi:10.1007/JHEP10(2024)190 [arXiv:2409.03840 [hep-ph]].
- [33] K. S. Babu, C. S. Fong and S. Saad, [arXiv:2508.14969 [hep-ph]].
- [34] B. Dutta, Y. Mimura and R. N. Mohapatra, *Phys. Lett. B* **603**, 35-45 (2004) doi:10.1016/j.physletb.2004.09.076 [arXiv:hep-ph/0406262 [hep-ph]].
- [35] D. Chang, R. N. Mohapatra and M. K. Parida, *Phys. Rev. Lett.* **52**, 1072 (1984) doi:10.1103/PhysRevLett.52.1072
- [36] W. Grimus and H. Kuhbock, *Eur. Phys. J. C* **51**, 721-729 (2007) doi:10.1140/epjc/s10052-007-0324-5 [arXiv:hep-ph/0612132 [hep-ph]].
- [37] I. Esteban, M. C. Gonzalez-Garcia, M. Maltoni, I. Martinez-Soler, J. P. Pinheiro and T. Schwetz, *JHEP* **12**, 216 (2024) doi:10.1007/JHEP12(2024)216 [arXiv:2410.05380 [hep-ph]]; NuFIT 6.0 (2024), www.nu-fit.org.
- [38] S. Davidson and A. Ibarra, *Phys. Lett. B* **535**, 25-32 (2002) doi:10.1016/S0370-2693(02)01735-5 [arXiv:hep-ph/0202239 [hep-ph]].
- [39] P. Di Bari and A. Riotto, *JCAP* **04**, 037 (2011) doi:10.1088/1475-7516/2011/04/037 [arXiv:1012.2343 [hep-ph]].
- [40] K. S. Babu, B. Bajc and S. Saad, *JHEP* **10**, 135 (2018) doi:10.1007/JHEP10(2018)135 [arXiv:1805.10631 [hep-ph]].